Bloch bound states in the radiation continuum in a periodic array of dielectric rods

Evgeny N. Bulgakov and Almas F. Sadreev
L.V. Kirensky Institute of Physics, 660036 Krasnoyarsk, Russia
(Received 24 August 2014; published 3 November 2014)

We consider an infinite periodic array of dielectric rods in vacuum with the aim to demonstrate three types of Bloch bound states in the continuum (BSCs): symmetry protected with a zero Bloch vector, embedded in one diffraction channel with nonzero Bloch vector, and embedded in two and three diffraction channels. The first and second types of the BSC exist for a wide range of material parameters of the rods, while the third occurs only at a specific value of the radius of the rods. We show that the second type supports the power flux along the array. In order to find BSCs we put forward an approach based on the expansion over the Hankel functions. We show how the BSC reveals itself in the scattering function when the singular BSC point is approached along a specific path in the parametric space.

DOI: 10.1103/PhysRevA.90.053801 PACS number(s): 42.25.Fx, 41.20.Jb, 42.79.Dj

I. INTRODUCTION

In 1929, von Neumann and Wigner [1] predicted the existence of discrete solutions of the single-particle Schrödinger equation embedded in the continuum of positive-energy states, bound states in the continuum (BSCs). Their analysis, examined by Stillinger and Herrick [2], was regarded for a long time as a mathematical curiosity because of certain spatially oscillating central symmetric potentials. That situation cardinally changed when Friedrich and Wintgen [3] formulated a generic two-level Fano-Anderson model and derived a condition for the BSC as a resonant state whose width tends to zero as at least one physical parameter varies continuously (see, also [4–6]). Currently, one can see a rapid growth in the number of publications, both theoretical and experimental, devoted to the BSCs in different physical systems [7–23].

The BSC can be classified by the mechanism responsible for the localization of waves [15,16]. The most obvious mechanism is related to the symmetry [7,11] when the continuum states and the BSCs have incompatable symmetries. The second mechanism is a Fabry-Perot resonator with the wave trapped between the mirrors as the distance between the mirrors is tuned. That mechanism was used in the system of quantum dots coupled by a wire [24,25] as well as in photonics [9,10,13,26,27]. The above-mentioned types of the BSC were extensively studied in different photonic structures and were experimentally observed [14,17–20]. The third mechanism is full destructive interference of two resonances, which was originally put forward by Friedrich and Wintgen [3] and later developed in Refs. [6,21]. It should be noted, however, that experimental observation of this type of BSC is difficult because it is necessary to vary material parameters [20]. Fourth, at some value of the parameters the coupling of a bound state of the closed system with the continuum channel can turn to zero accidentally, giving rise to the accidental BSC [16]. We speculate that this mechanism underlies the robust BSC observed in the photonic crystal slab [22,23]. In the present paper we consider a one-dimensional periodic array of GaAs cylindrical rods. We show that the array is capable of supporting multiple symmetry-protected Bloch BSCs. The Bloch BSC with a nonzero wave vector supports power flux. We also show that there are Bloch BSCs embedded into two and three continua.

II. BASIC EQUATIONS FOR ELECTROMAGNETIC WAVE SCATTERING BY A PERIODIC ARRAY OF RODS

The system under consideration is an infinitely long array of GaAs rods. The rods are infinitely long in the z direction, parallel to each other, and periodically spaced with distance h along the x axis on the x-y plane, as shown in Fig. 1. In what follows we take $h = 1$. We consider the scattering of transverse magnetic electromagnetic waves by this array. The scattering of plane waves by cylinders has been the subject of many investigations. Most difficulties in this connection are caused by multiple scattering by cylinders [28]. The problem was considered for the cases of two cylinders [29] and an infinite periodic row of cylinders [30,31], and a simple and tractable formulation was developed. In this section we present the basic equations of that theory for the reader's convenience (based on Ref. [31]).

Assume that the periodic array of rods is illuminated by a plane wave

$$\psi_{\rm inc}(x,y) = \sqrt{\frac{2}{|k_y|}} e^{i(k_x x + k_y y)},$$

where ψ is the electric field directed along the rods, $k_x = -k_0 \cos\varphi_i, k_y = -k_0 \sin\varphi_i, k_0 = \omega/c$, and φ_i defines the angle of incidence. The plane wave can be expanded over the Bessel functions,

$$\psi_{\rm inc}(r,\varphi) = \sqrt{\frac{2}{|k_y|}} \sum_m (-i)^m e^{im(\varphi-\varphi_i)} J_m(k_0 r) = \sum_m \psi_{{\rm inc},m} e^{im\varphi} J_m(k_0 r), \quad (1)$$

where

$$\psi_{{\rm inc},m} = \sqrt{\frac{2}{|k_y|}} (-i)^m e^{-im\varphi_i} = \sqrt{\frac{2}{|k_y|}} \left(\frac{ik_x + k_y}{k_0}\right)^m. \quad (2)$$

The scattered wave outside the rod is given by the Hankel functions

$$\Psi_s(r,\varphi) = \sqrt{\frac{2}{|k_y|}} \sum_m a_m \exp(im\varphi) H_m^{(1)}(k_0 r). \quad (3)$$

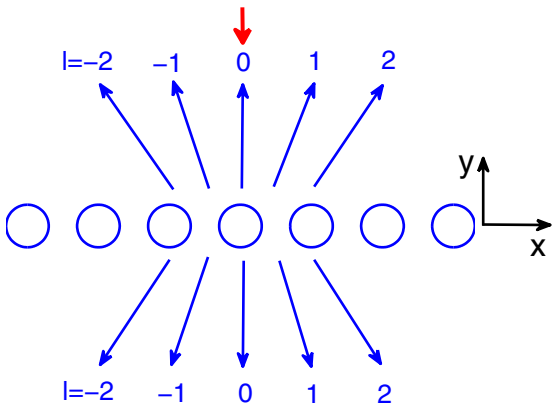

FIG. 1. (Color online) Cross section of a periodic array of parallel infinitely long rods illuminated by a plane wave [thick red (light gray) arrow]. The wave can be transmitted or reflected to discrete diffraction channels enumerated by integer l, shown by blue (dark gray) arrows.

The relation between incident and scattered waves is given by

$$a_m = \sum_n T_{mn}\psi_{\mathrm{inc},n}, \tag{4}$$

where the transition matrix has the following form:

$$T_{mn} = \delta_{mn}\frac{\sqrt{\epsilon}J_m'(qR)J_m(k_0R) - J_m'(k_0R)J_m(qR)}{H_m^{(1)'}(k_0R)J_m(qR) - \sqrt{\epsilon}J_m'(qR)H_m^{(1)}(k_0R)}, \tag{5}$$

where $q = \sqrt{\epsilon}k_0$ and ϵ is the permittivity of a rod of radius R. The scattering function is a sum of waves scattered from each rod:

$$\Psi_s(x,y) = \sqrt{\frac{2}{|k_y|}}\sum_j\sum_m a_{m,j}\exp(im\varphi_j)H_m^{(1)}(k_0r_j), \tag{6}$$

where (r_j,φ_j) is the local polar coordinate system whose origin is located in the center of the jth rod and $a_{m,j}$ denotes the amplitude of the field scattered from the jth rod. The periodicity of the structure requires the scattered field to satisfy the Bloch theorem:

$$\Psi_s(x+1,y) = \exp(ik_x)\Psi_s(x,y), \tag{7}$$

with k_x being the Bloch vector. Substituting Eq. (7) into Eq. (6), we have

$$\Psi_s(x,y) = \sqrt{\frac{2}{|k_y|}}\sum_j\sum_m \exp(ik_xj)a_m\exp(im\varphi_j)H_m^{(1)}(k_0r_j), \tag{8}$$

where $a_m = a_{m,0}$. The total wave function therefore is $\Psi = \Psi_{\mathrm{inc}} + \Psi_s$. Consequently, Eq. (7) defines the wave vectors of diffraction channels [27,31],

$$k_{y,l} = \sqrt{k_0^2 - k_{x,l}^2}, \quad k_{x,l} = k_x + 2\pi l,$$
$$l = 0, \pm1, \pm2, \quad \ldots. \tag{9}$$

The infinite periodic array of rods scatters the wave into only a number of directions defined by wave vectors $k_{x,l},k_{y,l}$. In the other words, the system under consideration supports only a finite number of continua or diffraction channels, denoted by integer l in Eq. (9), for which $k_{y,l}$ is real. The diffraction channel waves are given by

$$\psi_l^{r,t} = \sqrt{\frac{2}{k_{y,l}}}e^{ik_{x,l}x\pm ik_{y,l}y}. \tag{10}$$

Here indexes t,r imply the transmitted and reflected plane waves which are schematically shown in Fig. 1 by thin blue (dark gray) arrows.

Following Ref. [31], we introduce the aggregate matrix $\widehat{A}$, which relates the amplitudes $\Psi = \{\psi_{\mathrm{inc},m}\}$ in the expansion of the incident plane wave (1) to the amplitudes $\mathbf{a} = \{a_m\}$ of scattered wave (8),

$$\mathbf{a} = \widehat{A}\Psi_{\mathrm{inc}}. \tag{11}$$

That matrix could be considered an analog of the scattering matrix; however, there is an important difference. The latter connects the scattering channels denoted by l with the incident wave, while the former connects the amplitudes of the Hankel functions in the scattered wave with the incident wave.

For an infinite periodic array of rods multiple scattering events can be summated as follows [31]:

$$\widehat{A} = (1 - \widehat{T}\widehat{L})^{-1}\widehat{T} \tag{12}$$

where the $\widehat{T}$ matrix is given by Eq. (5) and

$$L_{n-m} = \sum_{l=1}^{\infty} H_{n-m}^{(1)}(lk_0h)[e^{ik_xl} + (-1)^{n-m}e^{-ik_xl}]. \tag{13}$$

Let us introduce components of waves transmitted and reflected in the lth diffraction channel,

$$\mathbf{v}_l^{(t,r)} = \sqrt{\frac{2}{k_{y,l}}}\left\{\left(\frac{ik_{x,l} \mp k_{y,l}}{k_0}\right)^m\right\}, \tag{14}$$

in terms of which we rewrite Eq. (11) in accordance with Eq. (2):

$$\mathbf{a} = \widehat{A}\mathbf{v}_0^{(t)}. \tag{15}$$

Then we have [31]

$$r_l = \left[\mathbf{v}_l^{(r)}\right]^+\mathbf{a}, \quad t_l = \delta_{l,0} + \left[\mathbf{v}_l^{(t)}\right]^+\mathbf{a}, \tag{16}$$

which are the reflection and transmission amplitudes for open channels, respectively. The scattering function (6) can be written as follows [31]:

$$\Psi_s(x,y) = \begin{cases}\sum_l r_l\psi_l^{(r)}(x,y) & \text{if} \quad y > 0,\\ \sum_l t_l\psi_l^{(t)}(x,y) & \text{if} \quad y < 0,\end{cases} \tag{17}$$

where both open and closed channels are summated.

III. CALCULATION OF BOUND STATES IN THE CONTINUUM

Typically, a plane wave is scattered by the array of rods into diffraction channels according to Eq. (15). However, there could be a unique case when the matrix $\widehat{A}$ in Eq. (15) is singular and the solution for the scattering wave exists irrespective of the incident-wave amplitude $\mathbf{v}_0^{(t)}$. As will be shown below, this unique solution is decoupled from the diffraction channels and localized near the array. This solution is the bound state

with the frequency embedded in the diffraction continua, i.e., a BSC. In this section we adapt the approach of the effective non-Hermitian Hamiltonian [32,33] to calculate a BSC in the periodic array of rods.

As can be seen from Eq. (15) the aggregate matrix $\widehat{A}$ must be singular for the BSC to exist. This matrix is not Hermitian, and similar to the approach of the effective Hamiltonian [34,35], it is fruitful to introduce the biorthogonal basis of the eigenvectors of the matrix

$$\widehat{\Lambda} = \widehat{A}^{-1} = \widehat{T}^{-1} - \widehat{L} \tag{18}$$

as follows:

$$\widehat{\Lambda}\mathbf{x}_f = \lambda_f \mathbf{x}_f, \quad \widehat{\Lambda}^{+}\mathbf{y}_f = \lambda_f^{*}\mathbf{y}_f, \quad \mathbf{y}_f^{+}\mathbf{x}_g = \delta_{fg}. \tag{19}$$

One can show that

$$\sum_f \mathbf{x}_f \mathbf{y}_f^{+} = 1, \quad \widehat{\Lambda}^{-1} = \sum_f \frac{\mathbf{x}_f \mathbf{y}_f^{+}}{\lambda_f}. \tag{20}$$

Then by using Eqs. (19) and (20) the scattering state in Eq. (15) can be expanded over the biorthogonal basis as follows:

$$\mathbf{a} = \sum_f \frac{\left(\mathbf{y}_f^{+}\mathbf{v}_0^{(t)}\right)\mathbf{x}_f}{\lambda_f}. \tag{21}$$

By substituting Eq. (21) into (16) we obtain the scattering amplitudes in the following form:

$$r_l = \sum_f \frac{W_{f,l}^{(r)}\widetilde{W}_{f,0}^{(t)}}{\lambda_f}, \quad t_l = \delta_{l,0} + \sum_f \frac{W_{f,l}^{(t)}\widetilde{W}_{f,0}^{(t)}}{\lambda_f}, \tag{22}$$

where we introduced the coupling constants between the fth eigenvector of the matrix Λ and the lth diffraction channel vector $\mathbf{v}_0^{(t)}$,

$$W_{f,l}^{(r,t)} = \left[\mathbf{v}_l^{(r,t)}\right]^{+}\mathbf{x}_f, \quad \widetilde{W}_{f,0}^{(t)} = \mathbf{y}_f^{+}\mathbf{v}_l^{(t)}. \tag{23}$$

Equations (22) are similar to those derived in Ref. [34].

The BSC occurs when at least one of the complex eigenvalues λ equals zero,

$$\widehat{\Lambda}\Phi_{\mathrm{BSC}} = 0. \tag{24}$$

Therefore, the BSC is, in fact, a null eigenvector. Next, Eqs. (22) show that for the scattering amplitudes to remain finite we have to imply the condition

$$\left[\mathbf{v}_l^{r,t}\right]^{+}\Phi_{\mathrm{BSC}} = 0. \tag{25}$$

This equation shows that the BSC is decoupled from all open diffraction channels and therefore does not leak into the radiation continuum.

IV. SYMMETRY-PROTECTED BSC

In what follows we take the dielectric constant of the rods $\epsilon = 12$ (GaAs rods). We briefly describe the numerical procedure to calculate the BSC function. In the first step the eigenvalue problem for the matrix Λ defined by Eqs. (13) and (18) is solved. Numerically, we truncate the rank of the matrix Λ by $|m| \leqslant 10$ to ensure sufficient accuracy. Then the eigenvector components a_m are substituted first into Eq. (16) and then into Eq. (17) to find the BSC wave function outside the rods. A summation over l includes only closed channels, i.e., evanescent modes. The BSC function inside the rods should be expanded over the Bessel functions, where the coefficients are calculated by means of matching the outside and inside functions on the boundary of the rods.

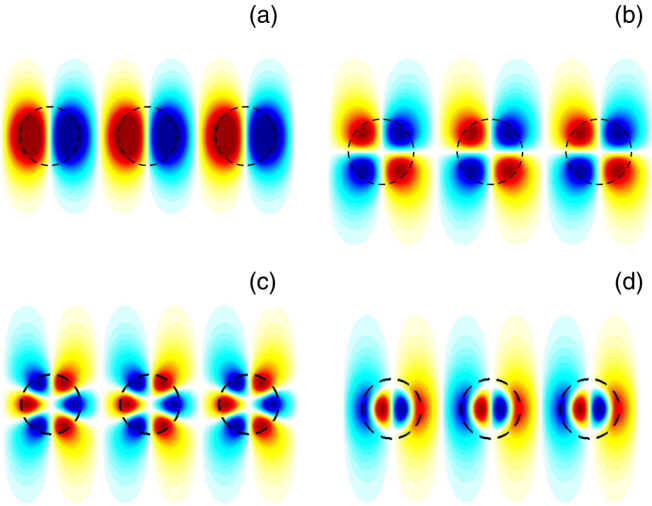

FIG. 2. (Color online) Patterns of the symmetry-protected BSCs which are solutions of Eq. (24) for $\epsilon = 12, R = 0.3$ and (a) $k_0 = h\omega/c = 2.542$, (b) $k_0 = 3.6467$, (c) $k_0 = 4.85$, and (d) $k_0 = 5.3125$. The array of rods is shown by dashed circles.

Let us assume that only diffraction channel $l = 0$ is open. Examples of Bloch states embedded in this channel are shown in Fig. 2 for $k_x = 0$; the pattern of the BSC in Fig. 2(a) was first presented by Shipman and Venakides [7]. We show that these Bloch BSCs are symmetry protected. For $k_x = 0,\pi$ the matrix $\widehat{\Lambda}$ has the property

$$\Lambda_{m,n} = \Lambda_{|m-n|}. \tag{26}$$

Let us introduce the operator which inverts the indexes of a_m,

$$\widehat{P}a_m = a_{-m}. \tag{27}$$

Then it follows from Eq. (26) that the operator $\widehat{P}$ commutes with the matrix $\widehat{\Lambda}$. Therefore, the eigenvectors of the matrix $\widehat{\Lambda}$ are only symmetric or antisymmetric relative to $m \to -m$; in particular, the same holds true for the BSC,

$$\Psi_{m,\mathrm{BSC}}^{s,a} = \pm\Psi_{-m,\mathrm{BSC}}^{s,a}, \tag{28}$$

where s and a stand for symmetric and antisymmetric states, respectively. For $k_x = 0,\pi$ an additional property arises, as can be seen from Eq. (13):

$$\Lambda_{|2m+1|} = 0. \tag{29}$$

That additional property allows us to split the BSCs into the following types. The BSCs of the first type have only odd components, $a_{2m}^{o} = 0$, while the BSCs of the second type have only even components, $a_{2m+1}^{e} = 0$. Thus, the BSCs for $k_x = 0,\pi$ can be split into four types: $(s,o),(s,e),(a,o),(a,e)$.

For diffraction channel $l = 0$ with $k_x = 0$ we have, from Eq. (14),

$$v_{l=0,m}^{(t)} = \sqrt{\frac{2}{k_{y,0}}}(-1)^m, \quad v_{l=0,m}^{(r)} = \sqrt{\frac{2}{k_{y,0}}}. \tag{30}$$

Substituting Eq. (30) into Eq. (25), we find that only two types of the BSCs, (a,o) and (a,e), are symmetry protected. Let us consider first the Bloch BSC which belongs to the type (a,o). Matching the solutions (8) on the boundary of the rod, we find the BSC wave-function interior of the $j = 0$ rod as follows:

$$\Phi(r,\varphi)^{(a,o)} = \sum_{m=1}^{\infty} A_{2m-1}(r)\cos(2m-1)\varphi, \tag{31}$$

with

$$A_m(r) = \frac{\frac{J_m(k_0R)}{T_{mm}} + H_m^{(1)}(k_0R)}{J_m(qR)} a_m J_m(qr), \tag{32}$$

where the property of the Bessel functions $J_{-m}(x) = (-1)^m J_m(x)$ was taken into account. One can see that the BSC function has the nodal line at $\varphi = \pi/2$, i.e., at $x = 0$. However, because the BSC is a Bloch wave, we obtain a periodical set of nodal lines at $x = 0, \pm1, \pm2, \ldots$. Note that the BSC does not exist only within the rods. Although there is no contribution of the $l = 0$ diffraction channel to scattering function (17) because $r_{l=0} = 0, t_{l=0} = 0$, there are contributions of closed evanescent diffraction channels with $l \neq 0$. According to Eq. (9), the dominant contribution $l = 1$ gives us the localization scale in the y direction as

$$y_{\mathrm{BSC}} \sim 1/\sqrt{4\pi^2 - k_0^2}. \tag{33}$$

The patterns of the antisymmetric odd Bloch BSC are shown in Figs. 2(a), 2(c), and 2(d).

For the antisymmetric even BSC (a,e) we have the following solution within the rods:

$$\Phi(r,\varphi)^{(a,e)} = \sum_{m=1}^{\infty} A_{2m}(r)\sin 2m\varphi, \tag{34}$$

which has the nodal lines at $\varphi = 0, \pi/2$. The numerically calculated pattern of this BSC is shown in Fig. 2(b). Thus, the antisymmetric Bloch BSC exists provided that the BSC frequency k_0 does not exceed the threshold of the next diffraction channels with $l \neq 0$. Figure 3 shows that all symmetry-protected BSCs from Fig. 2 coexist for a wide range of the radius of the rods.

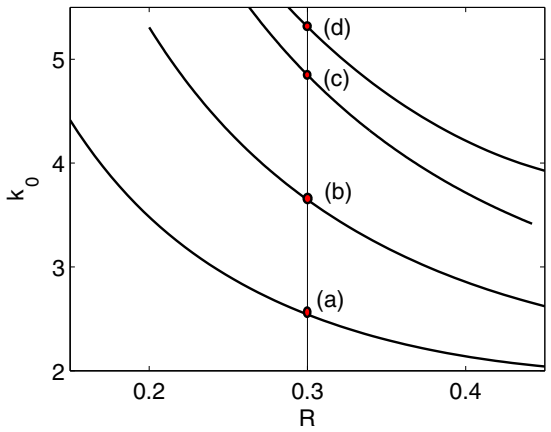

FIG. 3. (Color online) BSC frequencies $k_0 = \omega/c$ vs radius R for the BSCs shown in Fig. 2.

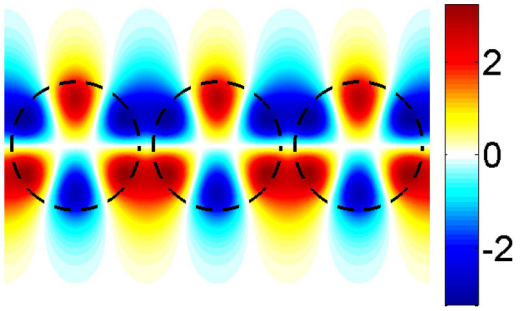

FIG. 4. (Color online) Real part of the symmetric odd Bloch BSC for $R = 0.4515, k_0 = 3.0887, k_x = 0$.

Next, we consider the symmetric odd BSC (s,o) in the diffraction channel $k_x = 0, l = 0$. Substituting Eqs. (30) and (28) into Eq. (25), we obtain

$$\left[\mathbf{v}_l^{r,t}\right]^+ \Phi^{(s,o)} = 2\sqrt{\frac{2}{k_{y,0}}} \sum_{m=1}^{\infty} \Phi_{2m-1}^{(s,o)}. \tag{35}$$

In contrast to the antisymmetric wave, the right-hand part of this equation can equal zero only accidentally as one varies the radius of the rods. The corresponding BSC function,

$$\Phi(r,\varphi)^{(s,o)} = \sum_{m=1}^{\infty} A_{2m-1}(r)\sin(2m-1)\varphi, \tag{36}$$

is presented in Fig. 4. This BSC has nodal lines at $y = 0$. The symmetric even BSC (s,e) wave function has the following form for $r < R$:

$$\Phi(r,\varphi)^{(s,e)} = \sum_{m=0}^{\infty} A_{2m}(r)\cos 2m\varphi. \tag{37}$$

However, for a given parameter $\epsilon = 12$ our computation revealed only the symmetric odd BSC. Thus, neither the odd nor even BSC can be classified as symmetry protected because of the necessity to adjust the right-hand part of Eq. (35) to zero.

V. THE BOUND STATES EMBEDDED IN TWO AND THREE DIFFRACTION CHANNELS

Now, we show that the BSC can exist even when more than one diffraction channel is open. This phenomenon was considered by Ndangali and Shabanov in the double arrays of dielectric rods [27]. They showed that tuning for BSC requires a higher dimensionality of the parametric space. In Ref. [16] we demonstrated that the BSC can be robust relative to a few open channels owing to the symmetry of the resonator. We show in this section that the present system can also support BSC embedded in a few diffraction channels. First, we assume that only two diffraction channels, $l = 0, k_{x,0} = k_x = \pi$ and $l = -1, k_{x,-1} = -\pi$, are open. The components of ingoing and outgoing waves (14) satisfy the following relationships:

$$v_{l=0,m}^{(r,t)} = \left[v_{l=-1,m}^{(r,t)}\right]^* = v_{l=-1,-m}^{(r,t)}. \tag{38}$$

In this case all symmetric properties established in Eqs. (28) and (29) still hold true. We start with the symmetric odd state (s,o) and consider its coupling with the channels (38)

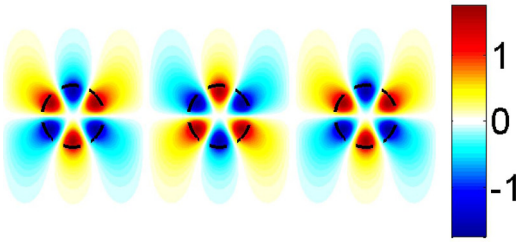

FIG. 5. (Color online) Real part of the (s,o) BSC wave function embedded in the open $l = 0, l = -1$ diffraction channels for $R = 0.2107, k_0 = 6.87, k_x = \pi$.

to establish the following equalities:

$$W_{l=0}^{(r,t)} = W_{l=-1}^{(r,t)}, \quad W_{l=0}^{(r)} = -W_{l=0}^{(t)}. \tag{39}$$

Here, for brevity we omitted the superscript (s,o). One can see that all coupling constants equal zero if $W_{l=0}^{(t)} = 0$, which can be fulfilled by varying the radius of the rod. Such a Bloch BSC function is shown in Fig. 5. For $\epsilon = 12$ we did not find the BSC for the other symmetry types, $(s,e),(a,o),(a,e)$. However, that does not mean that they are impossible for different ϵ.

Next, we consider the case of three open diffraction channels $l = 0, k_{x,0} = k_x = \pi$; $l = 1, k_{x,1} = \pi$; and $l = -1, k_{x,-1} = -\pi$, the maximum number of open channels with an embedded bound state. Our simulations show that the only the antisymmetric odd BSC (a,o) can exist, for which the symmetry establishes five equalities for six coupling constants:

$$W_{l=-1}^{(r,t)} = -W_{l=1}^{(r,t)}, \quad W_{l=1}^{(r)} = W_{l=1}^{(t)}, \quad W_{l=0}^{(r)} = W_{l=0}^{(t)} = 0. \tag{40}$$

Similar to the previous case, in order to cancel all couplings it is enough to fulfill $W_{l=1}^{(t)} = 0$. The last equality can be achieved by tuning the radius of the rods. The wave function within the rods has the following form:

$$\Phi(r,\varphi)^{(a,o)} = \sum_{m=1}^{\infty} A_{2m-1}(r)\cos(2m-1)\varphi. \tag{41}$$

The Bloch wave function is shown in Fig. 6. One can see that nodal lines at $x = 0, \pm 1/2, \pm 1, \ldots$ are similar to the antisymmetric odd Bloch BSC embedded in the first diffraction channel shown in Fig. 2.

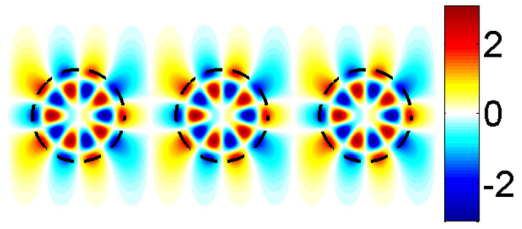

FIG. 6. (Color online) Real part of the (a,o) BSC wave function embedded in the three open diffractions channels: $l = 0, l = \pm 1$ for $R = 0.3193, k_0 = 9.876, k_x = 0$.

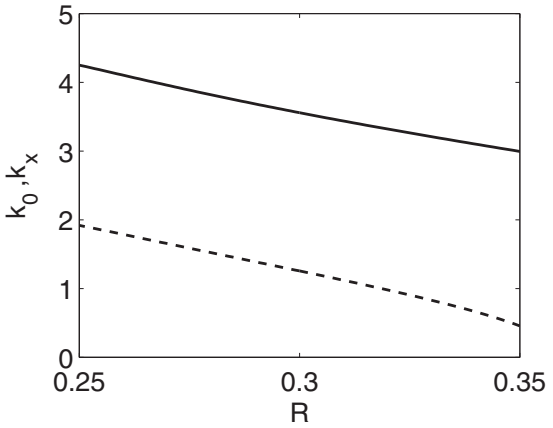

FIG. 7. k_x (solid line) and k_0 (dash line) vs the radius of rods R.

VI. BLOCH BSC WITH POYNTING VECTOR

Could the Bloch BSC occur at $\pi > k_x > 0$ in the continuum of free-space modes? This question was first answered positively by Porter and Evans [8], who considered acoustic trapping in an array of rods with a rectangular cross section. Later, Marinica *et al.* [10] demonstrated the existence of the Bloch BSC at $k_x > 0$ in two parallel dielectric gratings, and Ndangali and Shabanov [27] demonstrated its existence in two parallel arrays of dielectric rods. Each array has a transmission zero for the definite incident angle and frequency to form the Fabry-Pérot resonator that supports BSCs trapped between the "mirrors" [10]. In a single array of rods positioned on the surface of a bulk two-dimensional photonic crystal, multiple BSCs with $k_x \geqslant 0$ were considered by Wei *et al* [20]. That system can also be seen as a Fabry-Pérot resonator with the photonic crystal playing the role of the bottom mirror provided that the frequency is in the band gap. The periodic array of rods plays the role of top mirror at a certain frequency and radius of the rods. Such BSCs are one-dimensional Bloch surface states which do not leak into the radiation continuum [19]. The next important step was undertaken by Zhen *et al.* [36], who presented the Bloch BSC in a PhC slab with one-dimensional periodicity in x, where the Bloch BSC evolves with $k_x \neq 0, k_z = 0$ into the BSC with $k_x = 0, k_z \neq 0$ for decreasing slab thickness.

In the present paper we show that the electromagnetic Bloch BSC with $\pi > k_x > 0$ occurs in a periodic array of rods with a circular cross section as the result of zero coupling of the Bloch state with the diffraction channel at specific values of k_x and k_0. We stress that like in the systems described above [20,22,23], there is no need to tune the material parameters of the rods. The only condition is that the dielectric constant and the radius of the rods are large enough that only the $l = 0$ diffraction channel is open, as seen in Fig. 7. These Bloch BSCs are degenerate due to $k_x \to -k_x$ symmetry. Figure 8 shows the pattern of the BSC (real part) with the Poynting vector field, which indicates a power flux along the array. The diffraction channel parameters can be changed as one changes the radius of the rods, as shown in Fig. 7.

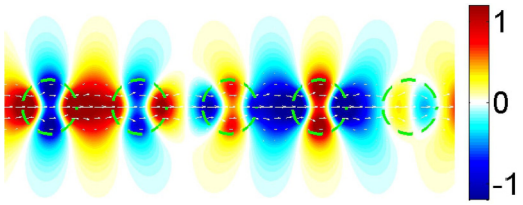

FIG. 8. (Color online) Real part of the propagating BSC for $R = 0.3, k_0 = 3.5577, k_x = 1.2556$. White arrows show the Poynting vector carrying the power current in the Bloch BSC.

VII. EMERGENCE OF THE BSC IN THE SCATTERING FUNCTION

It is clear that probing the BSC with a wave injected into a diffraction channel is impossible because the BSC is orthogonal to the channel. Nevertheless, one can show there is a path in the parametric space leading to the BSC point. Approaching the BSC point along this path reveals that the BSC is the dominant contribution in the scattering wave function (21). Assume that among all complex eigenvalues λ_f only one tends to zero, $\lambda_s \to 0$, while the others remain finite in the vicinity of the BSC point. In what follows we suppose that only one diffraction channel, $l = 0$, is open. Then we can write the singular part in the scattering wave (21) as follows:

$$\mathbf{a}_s = \frac{\left(\mathbf{y}_s^{+}\mathbf{v}_0^{(t,r)}\right)\mathbf{x}_s}{\lambda_s}, \tag{42}$$

where $\mathbf{x}_s$ is the eigenvector which tends to the null vector. We can also present the singular parts in the reflection and transmission amplitudes (16), i.e., the scattering matrix, as follows:

$$r_{sl} = \frac{W_{s,l}^{(r)}\widetilde{W}_{s,0}^{(t)}}{\lambda_s}, \quad t_{sl} = \frac{W_{s,l}^{(t)}\widetilde{W}_{s,0}^{(t)}}{\lambda_s}. \tag{43}$$

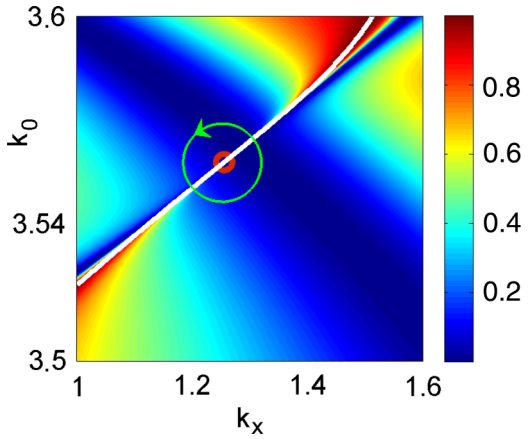

FIG. 9. (Color online) Transmittance vs k_0 and k_x for a wave incident to the array of dielectric rods shown in Fig. 1. The BSC point $k_0 = 3.5577, k_x = 1.2556, R = 0.3$ is shown by the red open circle.

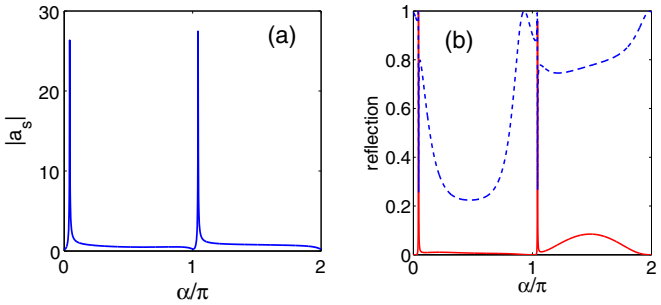

FIG. 10. (Color online) Behavior of (a) $|a_s|$ and (b) the reflection coefficient vs angular variable α for the encircling of the BSC point shown in Fig. 9.

Figure 9 shows the transmittance vs k_x and k_0. One can see a singular point where unit transmittance touches zero transmittance, which corresponds to the collapse of the Fano resonance [24]. This singular point k_{xs}, k_{0s} corresponds to the Bloch BSC shown in Fig. 8. To find the path leading to the BSC-like scattering wave, following Ref. [32], we consider the behavior of the scattering function as one encircles the singular point (shown in Fig. 9 by a green arrow). In Fig. 10 we plot the singular part in the scattering state (42) $|a_s|$ and the reflection coefficient $|r_{sl=0}|$ as a function of the angle variable α defined via $k_x - k_{xs} = \rho\cos\alpha, k_0 - k_{0s} = \rho\sin\alpha$, with $\rho = 0.1$. The angular behavior demonstrates sharp peaks. The smaller the radius ρ is, the sharper the peaks associated with the BSC are. Therefore, it follows that there is a path leading to the BSC-like scattering function. This path is shown by a white solid line in Fig. 9 which corresponds to the unit transmittance in the collapsing Fano resonance.

VIII. SUMMARY

In the present paper we used the approach presented in Ref. [31] for cylindrical rods. The approach is based on an expansion of incident and scattered waves over the Hankel or Bessel functions and has the advantage that the number of functions could be taken to be rather small. The symmetry of the system waves implies the symmetry selection rules for coefficients a_m in the expansion of the Bloch BSC. That results in four types of Bloch BSCs with wave vector $k_x = 0, \pi$, as classified in Sec. IV. In turn the symmetry restrictions for a_m are reflected in the space symmetry, as demonstrated in Fig. 2. It is important that the symmetry-protected Bloch BSC exists for a wide range of the material parameters of the rods. This symmetry property allows the existence of the Bloch BSC embedded in two and three diffraction channels, although at the price of tuning the radius of the rods. Such BSCs are presented in Figs. 4–6. The next interesting class of the Bloch BSC is the BSC with the nonzero Bloch wave vector shown in Fig. 8. This BSC carries a power flux along the array.

The BSCs exist at a selected point in the parametric space. So it might be thought that the BSCs are not important beyond that point. Following Ref. [32], we show that the scattering

wave function becomes BSC-like if one approaches the BSC point along the path where the transmission coefficient equals unity (see Figs. 9 and 10). This provides a path for experimental observation of the BSC.

ACKNOWLEDGMENTS

The work was supported by the Russian Science Foundation through Grant No. 14-12-00266. We acknowledge discussions with D. N. Maksimov.

[1] J. von Neumann and E. Wigner, Phys. Z. **30**, 465 (1929).
[2] F. H. Stillinger and D. R. Herrick, Phys. Rev. A **11**, 446 (1975).
[3] H. Friedrich and D. Wintgen, Phys. Rev. A **32**, 3231 (1985).
[4] A. Volya and V. Zelevinsky, Phys. Rev. C **67**, 054322 (2003).
[5] M. L. Ladron de Guevara, F. Claro, and P. A. Orellana, Phys. Rev. B **67**, 195335 (2003).
[6] A. F. Sadreev, E. N. Bulgakov, and I. Rotter, Phys. Rev. B **73**, 235342 (2006).
[7] S. P. Shipman and S. Venakides, Phys. Rev. E **71**, 026611 (2005).
[8] R. Porter and D. Evans, Wave Motion **43**, 29 (2005).
[9] E. N. Bulgakov and A. F. Sadreev, Phys. Rev. B **78**, 075105 (2008).
[10] D. C. Marinica, A. G. Borisov, and S. V. Shabanov, Phys. Rev. Lett. **100**, 183902 (2008).
[11] N. Moiseyev, Phys. Rev. Lett. **102**, 167404 (2009).
[12] N. Prodanovic, V. Milanovic, and J. Radovanovic, J. Phys. A **42**, 415304 (2009).
[13] E. N. Bulgakov and A. F. Sadreev, Phys. Rev. B **81**, 115128 (2010).
[14] T. Lepetit, E. Akmansoy, J.-P. Ganne, and J.-M. Lourtioz, Phys. Rev. B **82**, 195307 (2010).
[15] J. W. González, M. Pacheco, L. Rosales, and P. A. Orellana, Europhys. Lett. **91**, 66001 (2010).
[16] E. N. Bulgakov and A. F. Sadreev, Phys. Rev. B **83**, 235321 (2011).
[17] Y. Plotnik, O. Peleg, F. Dreisow, M. Heinrich, S. Nolte, A. Szameit, and M. Segev, Phys. Rev. Lett. **107**, 183901 (2011).
[18] G. Corrielli, G. Della Valle, A. Crespi, R. Osellame, and S. Longhi, Phys. Rev. Lett. **111**, 220403 (2013).
[19] S. Weimann, Y. Xu, R. Keil, A. E. Miroshnichenko, A. Tünnermann, S. Nolte, A. A. Sukhorukov, A. Szameit, and Yu. S. Kivshar, Phys. Rev. Lett. **111**, 240403 (2013).
[20] C. W. Hsu, B. Zhen, S.-L. Chua, S. G. Johnson, J. D. Joannopoulos, and M. Soljačič, Light Sci. Appl. **2**, 1 (2013).
[21] E. N. Bulgakov and A. F. Sadreev, Opt. Lett. **39**, 5212 (2014).
[22] C. W. Hsu, B. Zhen, J. Lee, S.-L. Chua, S. G. Johnson, J. D. Joannopoulos, and M. Soljacic, Nature (London) **499**, 188 (2013).
[23] Y. Yang, C. Peng, Y. Liang, Z. Li, and S. Noda, Phys. Rev. Lett. **113**, 037401 (2014).
[24] C. S. Kim, A. M. Satanin, Y. S. Joe, and R. M. Cosby, Phys. Rev. B **60**, 10962 (1999).
[25] I. Rotter and A. F. Sadreev, Phys. Rev. E **69**, 066201 (2004); **71**, 046204 (2005).
[26] S. Fan, P. R. Villeneuve, J. D. Joannopoulos, M. J. Khan, C. Manolatou, and H. A. Haus, Phys. Rev. B **59**, 15882 (1999).
[27] R. F. Ndangali and S. V. Shabanov, J. Math. Phys. **51**, 102901 (2010); Proc. SPIE **8808**, 88081F (2013).
[28] V. Twersky, J. Acoust. Soc. Am. **24**, 42 (1952); J. Appl. Phys. **23**, 407 (1952).
[29] J. W. Young and J. C. Bertrand, J. Acoust. Soc. Am. **58**, 1190 (1975).
[30] C. M. Linton and P. McIver, J. Eng. Math. **30**, 661 (1996).
[31] D. Maystre, S. Enoch, and G. Tayeb, in *Electromagnetic Theory and Applications for Photonic Crystals*, edited by K. Yasumoto (Taylor and Francis, Boca Raton, FL, 2006).
[32] E. N. Bulgakov, K. N. Pichugin, A. F. Sadreev, and I. Rotter, JETP Lett. **84**, 430 (2006).
[33] E. N. Bulgakov, I. Rotter, and A. F. Sadreev, Phys. Rev. A **75**, 067401 (2007).
[34] A. F. Sadreev and I. Rotter, J. Phys. A **36**, 11413 (2003).
[35] J. Okołowicz, M. Płoszajczak, and I. Rotter, Phys. Rep. **374**, 271 (2003).
[36] B. Zhen, C. W. Hsu, L. Lu, A. D. Stone, and M. Soljačić, arXiv:1408.0237.